Interfering Entangled Photons of Different Colors

T. S. Larchuk and R. A. Campos
Departments of Electrical Engineering and Applied Physics, Columbia University, New York, New York 10027

J. G. Rarity, P. R. Tapster, and E. Jakeman
Defense Research Agency, Royal Signals and Radar Establishment, Great Malvern, Worcester WR14 3PS, United Kingdom

B. E. A. Saleh
Department of Electrical and Computer Engineering, University of Wisconsin, Madison, Wisconsin 53706

M. C. Teich
Columbia Radiation Laboratory, Departments of Electrical Engineering and Applied Physics, Columbia University, New York, New York 10027
(Received 6 April 1992; revised manuscript received 11 December 1992)

We have observed unusual second- and fourth-order interference patterns when entangled photons with center-wavelength differences ≈ 40 nm are mixed together at single or dual Mach-Zehnder interferometers. The difference frequency of the photons appears directly in the spectrum of the coincidence rate. This phase-sensitive behavior can reveal center-frequency differences from zero to hundreds of THz.

PACS numbers: 42.50.Dv, 07.60.Ly

We report the observation of unusual interference patterns arising when highly nondegenerate photon pairs (i.e., photons of different colors) are fed into single and dual Mach-Zehnder interferometers (MZIs). We employ pair photons generated by parametric down-conversion, which are coincident in time and strongly linked in energy as a result of energy conservation inherent in their creation [1]. In the single MZI configuration, the paths of the pair beams have full spatial overlap (FSO) within the interferometer [Fig. 1(a)]. A simple adjustment to one of the mirrors in our apparatus results in a dual MZI, in which the paths of the pair beams have no spatial overlap (NSO) [Fig. 1(b)]. The interference is manifested as the path-length difference of the interferometer is swept from zero separation to very large separations.

Second- and fourth-order interference are simultaneously present in our experiments; the former is measured by counting the number of photons at the output of a single interferometer port whereas the latter is determined by measuring the coincidence rate at two output ports.

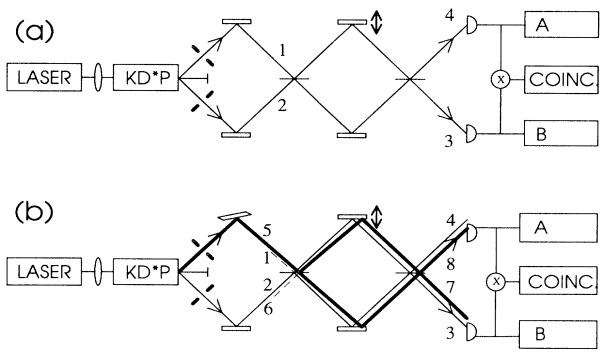

FIG. 1. Schematic diagram of the experimental apparatus.

We compare the interference patterns we observe with those calculated for coherent-state wave packets with similar spectral widths. The second-order pattern at any of the output ports is predicted to be the same for both coherent-state wave packets and pair photons. Oscillations at one, or both, of the center frequencies of the photons are expected (depending on whether there is NSO or FSO), and these die away when the path-length difference exceeds the second-order coherence length.

The fourth-order interference patterns for both pair photons and coherent-state wave packets are rich in structure, but differ in essential ways. For short path-length differences, spectral components at the difference ($\omega_d = |\omega_1 - \omega_2|$) and sum ($\omega_s = \omega_1 + \omega_2$) of the center frequencies of the photons appear in the coincidence rates resulting from either pair photons or coherent-state wave packets, for both FSO and NSO; in the case of NSO, individual spectral components at ω_1 and ω_2 are also present. A striking distinction for the pair-photon case is the continuation of sum- (pump-) frequency oscillations for path-length differences that extend well beyond the second-order coherence lengths. This is a nonlocal quantum effect. Although a number of experiments have revealed the existence of these oscillations for degenerate photons [1,2], our experiments confirm their presence for down-converted photons with large center-frequency differences. These nonclassical effects also allow us to experimentally determine the extent to which quantum entanglement is adhered to in the down-conversion process.

Yet other unique properties of the fourth-order interference patterns result from the coincidence properties of correlated photon pairs. The ratio of the coincidence-to-singles rate is limited only by the efficiency of the optical system and can be very high. The use of a short coincidence gate ensures that only one pair of photons at a

time is observed in pair-photon coincidence experiments. However, for coherent-state wave packets, coincidences arising from the detection of two photons of the same color are possible. For FSO, this leads to spectral components in the coincidence rate centered at $2\omega_1$ and $2\omega_2$, in sharp contrast to the pair-photon results.

A schematic diagram of the experimental setup is shown in Fig. 1. The 30-mW, 406.7-nm line of a krypton-ion laser (the pump of fixed wavelength) is focused onto a 15-mm-long deuterated potassium dihydrogen phosphate (KD^*P) crystal oriented for type-I (ooe) phase matching at 90° incidence to the crystal's optic axis. Unconverted pump photons pass straight through the crystal and into a beam dump. Down-converted photons emerge at an angle to the pump beam, with degenerate photons emerging symmetrically in a cone with a half angle of roughly 14°; however, for this experiment we use nondegenerate (different center frequency) photons, which emerge asymmetrically in accordance with the phase-matching condition. With apertures of about 2 mm diameter, we selected out desired nondegenerate photon pairs with center frequencies around 800 and 840 nm. The photons were then directed, by mirrors, into the two input ports of the interferometer. The actual experiments made use of a folded Mach-Zehnder interferometer in which the beams were redirected onto a lower portion of the same beam-splitter cube by two corner-cube prisms. By adjusting the angle of one of the input mirrors, the photons' paths within the interferometer could be made to have either FSO [Fig. 1(a)], partial spatial overlap, or NSO [Fig. 1(b)]. For the purposes of the experiments considered here, the NSO case is equivalent to sending each photon into a separate interferometer. Two passively quenched avalanche-photodiode counting detectors are located at the output ports of the interferometer. The output pulses from the detectors are counted for 1 s to provide a measure of the rate of photon detections at each of the ports, and the sequence of standardized pulses from the two detectors are passed through a 10-ns AND gate and counted for 1 s to provide a measure of the coincidence rate.

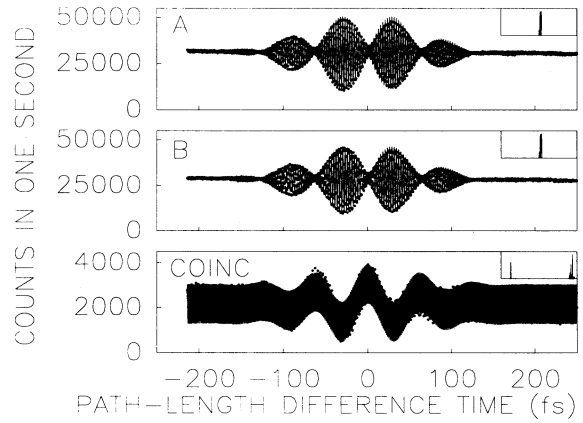

FIG. 2. Results of a scan of the Mach-Zehnder interferometer with full spatial overlap (FSO) of the beams. The dots are data points and the solid curves are fits of the theory to the data. The insets in the upper right-hand corners of each panel are the spectra of the interference patterns.

In Fig. 2 we present the results when the interferometer is adjusted for FSO [Fig. 1(a)]. The upper panel shows the counts recorded by detector A at output port 4, the middle panel shows the counts recorded by detector B at output port 3, and the lower panel shows the coincidence counts. The dots in the figures represent raw data. All of the data are collected simultaneously. Spectra of the interference patterns are shown in the upper right-hand corner of each panel. In Fig. 3 we present the results when the interferometer is adjusted for NSO [Fig. 1(b)].

To compare these experimental results with theoretical predictions, we consider the state of the light at the inputs to the interferometer [3]

$$|\Psi_{ij}\rangle = \int_0^\infty \int_0^\infty \zeta(\omega,\omega')|1_{i\omega}\rangle|1_{j\omega'}\rangle\, d\omega\, d\omega' , \qquad (1)$$

which describes entangled photons generated by parametric down-conversion and excited into field modes i and j. The quantity $\zeta(\omega,\omega')$ is a joint complex amplitude characterizing a joint Gaussian spectral density function $|\zeta(\omega,\omega')|^2$ with center frequencies ω_1 and ω_2, marginal spectral widths σ, and correlation parameter $\eta = -1$. The results we present here are for nondegenerate photons with $\omega_d > 2\sigma$. As illustrated in Fig. 1, $(i,j) = (1,2)$ for the case of FSO, whereas $(i,j) = (5,2)$ for NSO. Vacuum fields at appropriate ports are accounted for in the theory.

In the FSO case, we arrive at expressions for the photon singles-detection rates R_3 and R_4, and the photon coincidence-detection rate R_{34}, expected to be observed in an experiment as the path-length-difference time τ is swept [3]:

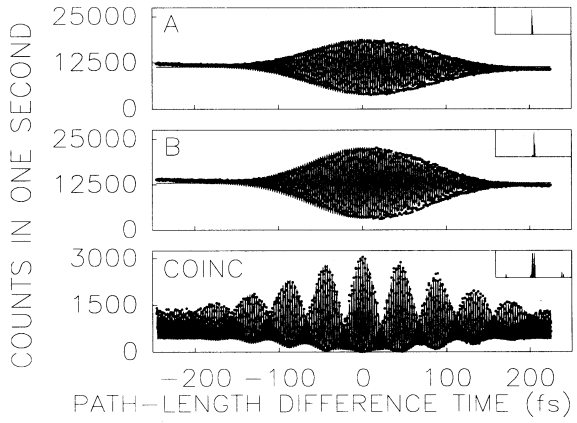

FIG. 3. Results of a scan of the Mach-Zehnder interferometer with no spatial overlap (NSO).

$$R_3=\frac{N_3}{2}+\frac{N_3V_3}{4}\exp(-\sigma^2\tau^2/2)[\cos(\omega_1\tau)-\cos(\omega_2\tau)]\,, \tag{2}$$

$$R_4=\frac{N_4}{2}-\frac{N_4V_4}{4}\exp(-\sigma^2\tau^2/2)[\cos(\omega_1\tau)-\cos(\omega_2\tau)]\,, \tag{3}$$

$$R_{34}=\frac{N_{34}}{2}+\frac{N_{34}V_{34}}{4}\times[\exp(-2\rho^2\sigma^2\tau^2)\cos(\omega_d\tau)+\cos(\omega_s\tau)]\,. \tag{4}$$

By contrast, in the case of NSO, the analogous results turn out to be

$$R_3=\frac{N_3}{2}-\frac{N_3V_3}{2}\exp(-\sigma^2\tau^2/2)\cos(\omega_2\tau)\,, \tag{5}$$

$$R_8=\frac{N_8}{2}-\frac{N_8V_8}{2}\exp(-\sigma^2\tau^2/2)\cos(\omega_1\tau)\,, \tag{6}$$

$$R_{38}=\frac{N_{38}}{4}-\frac{N_{38}V_{38}}{4}\exp(-\rho^2\sigma^2\tau^2/2)\times[\cos(\omega_1\tau)+\cos(\omega_2\tau)]+\frac{N_{38}V_{38}}{8}\times[\exp(-2\rho^2\sigma^2\tau^2)\cos(\omega_d\tau)+\cos(\omega_s\tau)]\,. \tag{7}$$

In these equations, the parameters N account for the number of trials conducted in each second during an experiment and for the quantum efficiencies of the detectors, the parameters V (which range from 0 to 1) accommodate imperfections and misalignments within the interferometer that reduce the visibility of the interference oscillations, and the parameter ρ (which also ranges from 0 to 1) accounts for geometrical effects that reduce the fourth-order bandwidths relative to those of second order (e.g., the finite spatial extent of the down-converter source [4] and the misalignment of apertures from their ideal conjugate positions).

These theoretical expressions are plotted as the solid curves in Figs. 2 and 3. The upper and middle panels of Fig. 3 for NSO display the shapes of the observed individual photon wave packets, justifying our assumption that they are approximately Gaussian [see Eqs. (5) and (6)]. Accordingly, each of the spectra shows a peak at the center frequency of one of the photons. The upper and middle panels of Fig. 2, in contrast, are sums of the second-order interference patterns of the two individual photons, so that the spectra each show two peaks at the center frequencies of both photons [see Eqs. (2) and (3)].

The theoretical and experimental fourth-order interference patterns for the case of FSO, shown in the lower panel of Fig. 2, are in remarkably good agreement. The experimental spectrum clearly reveals the sum and difference frequencies of the two photons [see Eq. (4)]. We have used the sum frequency as the starting point in the analysis of our data, taking it to correspond to the 406.7-nm wavelength of our krypton-ion laser pump. The parameter values determined by fitting Eqs. (2), (3), and (4) to the data points in Fig. 2 are $N_3=61724$, $N_4=56842$, $N_{34}=4320$, $V_3=0.72$, $V_4=0.72$, $V_{34}=0.82$, $\omega_1=2.260\times10^{15}$ rad/s, $\omega_2=2.359\times10^{15}$ rad/s, $\sigma=1.606\times10^{13}$ rad/s, $\omega_d=9.9\times10^{13}$ rad/s, and $\rho=0.5$, with $\omega_s=4.6316\times10^{15}$ rad/s. Using the relationships $\nu=\omega/2\pi$ and $\lambda=c/\nu$, where ν and λ represent the center frequency and wavelength of a photon, respectively, and c is the speed of light, we calculate that $\nu_1=359.7$ THz, $\nu_2=375.4$ THz, $\lambda_1=833.3$ nm, and $\lambda_2=798.5$ nm. The difference wavelength in this case is ≈35 nm and the difference frequency is 15.7 THz; however, from the spectra we can infer that frequency differences up to the frequency of the pump, 737.1 THz, are in principle measurable. Note that $\omega_d/2\sigma=3.082$ so that the nondegeneracy criterion required for the validity of the form of the equations presented here is satisfied [3].

The theoretical and experimental fourth-order interference patterns for NSO, shown in the lower panel of Fig. 3, are also in excellent agreement. The experimental spectrum contains the sum and difference as well as the center frequencies of each of the photons separately [see Eq. (7)]. The parameter values determined by fitting Eqs. (5), (6), and (7) to the data points in Fig. 3 are $N_3=22747$, $N_8=25945$, $N_{38}=3154$, $V_3=0.66$, $V_8=0.76$, $V_{38}=0.96$, $\omega_1=2.379\times10^{15}$ rad/s, $\omega_2=2.239\times10^{15}$ rad/s, $\sigma=1.582\times10^{13}$ rad/s, $\omega_d=1.40\times10^{14}$ rad/s, and $\rho=0.6$, again with $\omega_s=4.6316\times10^{15}$ rad/s. In this experiment we obtain $\nu_1=356.3$ THz, $\nu_2=378.7$ THz, $\lambda_1=841.2$ nm, and $\lambda_2=791.7$ nm, with a difference wavelength ≈50 nm. The frequency difference observed in this experiment was about 22 THz, with an accuracy of about 1 part in 10^6, but far greater accuracies are in principle possible. Note that $\omega_d/2\sigma=4.425$, again satisfying the nondegeneracy criterion.

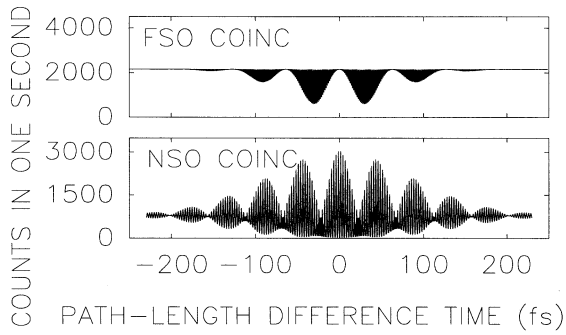

FIG. 4. Calculated fourth-order interference patterns for independent coherent-state wave packets at the inputs to the interferometer. The upper panel, calculated from Eq. (8), is for FSO (compare with the lower panel in Fig. 2). The lower panel, calculated from Eq. (9), is for NSO (compare with the lower panel in Fig. 3).

The coincidence efficiency of our experiments (i.e., the ratio of the coincidence rate to the singles rate) is $\approx 10\%$, about an order of magnitude greater than that achieved by other researchers, principally because of the high photon-detection efficiency of our apparatus ($\approx 35\%$). Unexpectedly, a low-visibility sum-frequency pattern is observed in the singles rate at large path-length differences. This apparent anomaly arises because of the high detection efficiency coupled with the detector's dead time. At fourth-order interference-pattern minima, photon pairs arrive at the same output port of the interferometer (randomly selected for each pair), where they cannot be resolved by the detector and thus cause a decrease in the mean count rate.

Were independent coherent-state wave packets presented as inputs to the interferometer, we would obtain second-order results identical to those provided in Eqs. (2), (3), (5), and (6). The fourth-order interference patterns in Eqs. (4) and (7), however, are unique to entangled states such as those generated by parametric down-conversion and described in Eq. (1). For coherent light at the input to the interferometer with FSO we obtain, instead of Eq. (4),

$$R_{34}^{(\mathrm{coh})}=\frac{N_{34}}{2}+\frac{N_{34}V_{34}}{8}\exp(-\rho^2\sigma^2\tau^2)[-\tfrac{1}{2}\cos(2\omega_1\tau)-\tfrac{1}{2}\cos(2\omega_2\tau)-1+\cos(\omega_d\tau)+\cos(\omega_s\tau)]\,, \tag{8}$$

whereas for coherent light into the interferometer with NSO we obtain, instead of Eq. (7),

$$R_{38}^{(\mathrm{coh})}=\frac{N_{38}}{4}-\frac{N_{38}V_{38}}{4}\exp(-\rho^2\sigma^2\tau^2/2)[\cos(\omega_1\tau)+\cos(\omega_2\tau)]+\frac{N_{38}V_{38}}{8}\exp(-\rho^2\sigma^2\tau^2)[\cos(\omega_d\tau)+\cos(\omega_s\tau)]\,. \tag{9}$$

Equation (8) is plotted in the upper panel of Fig. 4 while Eq. (9) is plotted in the lower panel. The parameters used in these plots are identical to those used in plotting the curves in the lower panels of Figs. 2 and 3.

For FSO, the fourth-order interference patterns are distinctly different for coherent-state wave packets (top panel of Fig. 4) and entangled photon pairs (bottom panel of Fig. 2). There are two principal distinctions: (i) sum-frequency oscillations for path-length differences exceeding the second-order coherence length are absent for coherent-state inputs (because they are not entangled), and (ii) the pattern assumes a rectified shape because of the presence of double-frequency components (corresponding to the absorption of one photon at each detector, but with both arising from one of the beams). In contrast, these double-frequency components do not appear in the NSO interference pattern because each coherent beam impinges on a different detector, thereby precluding pairs of photons from only one of the beams registering as coincidences. As a result, the NSO fourth-order patterns for coherent-state wave packets (bottom panel of Fig. 4) and entangled photon pairs (bottom panel of Fig. 3) are quite similar. However, as for the case of FSO, they differ in that sum-frequency oscillations at large path-length differences do not appear for coherent-state inputs.

It is clear that the data are in accord with the entangled-photon-pair results. In fact, using a generalized form of Eq. (4) valid for an arbitrary value of the parameter η [3], we determined that this parameter is very close to -1 ($-1\leq\eta\leq-0.99998$). Thus, essentially 100% of the coincidences arise from entangled photon pairs.

The center-frequency differences observed in our experiments (≈ 20 THz) are a result of the particular locations of our apertures. There is nothing to prevent us from choosing these arbitrarily (subject to their positions being conjugate), and thereby from observing center-frequency differences that in principle range from zero to hundreds of THz. As in the zero-frequency (degenerate) case examined previously [1], these measurements can be efficiently carried out in harsh environments (e.g., in the presence of copious amounts of background light). It appears that the NSO configuration is superior to the FSO configuration for this purpose, even though the throughput is a factor of 2 lower; this is because no joint adjustment of the beams is necessary. Indeed the "visibility" of the NSO interference pattern in the vicinity of $\tau=0$ is remarkably high ($V_{38}=0.96$) (bottom panel of Fig. 3).

This work was supported by the Joint Services Electronics Program through the Columbia Radiation Laboratory, by an AT&T Foundation grant to T.S.L. and M.C.T., and by NATO Collaborative Research Grant No. CGR:910571 to J.G.R. and M.C.T.

[1] J. G. Rarity, P. R. Tapster, E. Jakeman, T. Larchuk, R. A. Campos, M. C. Teich, and B. E. A. Saleh, Phys. Rev. Lett. **65**, 1348 (1990).

[2] Z. Y. Ou, X. Y. Zou, L. J. Wang, and L. Mandel, Phys. Rev. A **42**, 2957 (1990); Z. Y. Ou, X. Y. Zou, L. J. Wang, and L. Mandel, Phys. Rev. Lett. **65**, 321 (1990); P. G. Kwiat, W. A. Vareka, C. K. Hong, H. Nathel, and R. Y. Chiao, Phys. Rev. A **41**, 2910 (1990); J. D. Franson, Phys. Rev. A **44**, 4552 (1991); J. G. Rarity and P. R. Tapster, Phys. Rev. A **45**, 2052 (1992); J. Brendel, E. Mohler, and W. Martienssen, Phys. Rev. Lett. **66**, 1142 (1991).

[3] R. A. Campos, B. E. A. Saleh, and M. C. Teich, Phys. Rev. A **42**, 4127 (1990).

[4] J. G. Rarity and P. R. Tapster, Phys. Rev. A **41**, 5139 (1990).